Phased array element shapes for suppressing grating lobes

F. Joseph Pompei[a] and Shi-Chang Wooh[b]
Massachusetts Institute of Technology, Cambridge, Massachusetts 02139

(Received 7 August 2001; revised 28 November 2001; accepted 17 December 2001)

Most techniques for suppressing grating lobes in phased arrays while relaxing the interelement spacing requirement involve redistributing array elements in sparse aperiodic patterns, or varying the transmit-receive beam patterns. An alternative is presented which uses oversized array elements to eliminate grating lobes as a direct consequence of the element shape. It is shown that by using carefully shaped, overlapping elements, maximum scan angle can be exchanged for a reduced interelement spacing requirement. © *2002 Acoustical Society of America.*
[DOI: 10.1121/1.1460924]

PACS numbers: 43.20.Rz, 43.20.Bi [DEC]

I. INTRODUCTION

Phased arrays have long been used for both transmission and reception of sound waves in a variety of acoustic applications. Ultrasonics, in particular, has a long history of phased arrays for applications such as underwater acoustics, medical imaging, ultrasonic therapy, and nondestructive evaluation (NDE).

The most important parameters affecting the cost and performance of a phased array system are the number of elements and the interelement spacing necessary to provide a desired steering response. In a traditional periodic array, an interelement spacing of less than half the wavelength ($\lambda/2$) is required to mitigate detrimental grating lobes.[1,2] Because the main lobe width is dependent only on the spatial extent of the array, the generation of a narrow beam will usually require a large array and an inordinate number of individually driven elements.

Various methods have been proposed to relax the interelement spacing requirement to create sparse arrays of fewer elements with reduced grating lobes. Because the grating lobes are a result of the periodicity of the element positions, they can be reduced through the use of a random or aperiodic distribution of elements, although at the expense of a reduced dynamic range.[1,3,4] Others have proposed using different element patterns for transmit versus receive modes,[5–8] or by relying on very short pulses.[9] While these techniques are generally successful, they are applicable only for pulse-echo systems, not continuous wave systems, such as loudspeakers, microphone arrays, or parametric audio sources.[10]

Most of these earlier studies involve addressing the position and distribution of the individual elements, but little attention has been paid to the characteristics of the elements themselves. It is well known[11] that the directivity envelope pattern is wholly determined by the shape and size of the constituent elements, so it is logical that the element shape can be used to control various steering characteristics. In particular, elements larger than the interelement spacing will narrow the directivity envelope substantially, naturally suppressing grating lobes for a limited steering angle. Aspects of this technique have been explored for antenna arrays,[12] but it has received little attention in the context of acoustics or ultrasonics.

In this study, it is shown that overlapping arrays of various oversized elements can be used to suppress grating lobes, and allow a relaxed interelement spacing requirement for a limited steering angle. A brief review of relevant phased array theory is introduced, followed by a consideration of overlapped arrays of common element shapes which suppresses grating lobes to some extent, at the expense of a nonuniform main lobe amplitude. An optimal element shape is then developed, which effectively squelches grating lobes without influencing the main lobe. For convenience, only one-dimensional arrays are considered in this paper, although most of the techniques may also be applicable to higher-dimensional arrays.

II. BASIC THEORY

The far-field response of an arbitrary source condition can be derived using Huygen's principle, which may then be tailored to describe the specific case of a traditional linear array with uniformly spaced elements. This is largely based on the analysis given in Refs. 1, 2, and 11.

A. Huygen's principle

Huygen's principle states that any wave-producing source can be modeled as an infinite number of individual sources distributed identically to the original source. A pulsating point source radiates energy in spherical waves described by the equation

$$p_{\text{point}}(R) = \frac{dp_0}{R} e^{j(\omega t - kR)}, \tag{1}$$

where dp_0 is the source amplitude, R is the distance from the source to the point of interest, ω is the driving frequency, k is the wave number, and j is the unit imaginary number.

With an infinite baffle assumption, modeling a one-dimensional source with arbitrary source amplitude distribution $s(x)$, as shown in Fig. 1, results in the pressure distribution in an integral form:

$$p(r,\theta) = e^{j\omega t} \int \frac{s(x)}{R} e^{-jkR}\, dx. \tag{2}$$

[a]Media Laboratory, Massachusetts Institute of Technology, Room E15-492, 20 Ames St., Cambridge, MA 02139. Electronic mail: pompei@media.mit.edu
[b]Department of Civil and Environmental Engineering, Massachusetts Institute of Technology, Room 1-272, 77 Massachusetts Avenue, Cambridge, MA 02139. Electronic mail: scwooh@mit.edu

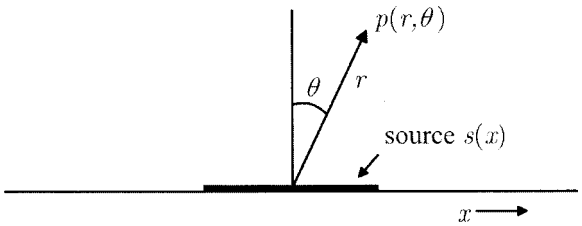

FIG. 1. The geometry of the one-dimensional source under consideration.

The source amplitude $s(x)$ is the contribution of source element dx to the pressure at point p, and relates to the source's normal vibration velocity amplitude $u(x)$ as $s(x) = (\rho_0 \omega/2\pi)u(x)$.

The $e^{j\omega t}$ term may be omitted for a linear and nondispersive system, and R can be approximated as

$$R = (r^2 + x^2 - 2rx \sin\theta)^{1/2} \approx r - x \sin\theta + \frac{x^2}{2r}. \tag{3}$$

Substituting this approximation into the integral gives

$$p(r,\theta) = \frac{1}{r} e^{-jkr} \int s(x) e^{jkx \sin\theta} e^{-jk(x^2/2r)}\, dx. \tag{4}$$

The last factor in the integral is significant only for small r, when $r \ll 1/2kx^2$, the Fresnel distance. The other factors are not dependent on r, and therefore it describes the pressure in the *far field* of the source. For simplicity, this analysis will address only far-field effects, limiting the extent of the array to those dimensions for which this approximation is satisfied.

B. Fourier analysis

If the change in variables $x' = x/\lambda$ and $\beta = \sin\theta$ is made while disregarding the amplitude scaling with r, the integral describing the far-field directivity becomes

$$H(\beta) = \int s(x') e^{j2\pi x' \beta}\, dx'. \tag{5}$$

This is the Fourier transform of the source distribution function scaled by $1/\lambda$. This important result makes the analysis of the far field straightforward and intuitive.

As an alternative, which is more suitable for discrete Fourier transform (DFT) simulation, one can substitute $\Omega = \beta/\lambda$, and arrive at

$$H\left(\frac{\beta}{\lambda}\right) = f(\Omega) = \int s(x) e^{j2\pi\Omega x}\, dx. \tag{6}$$

In this case, the scaling with λ is taken *after* the Fourier transform, so that downsampling prior to taking the DFT is not necessary.

Simulation Steps:

(1) Given the source distribution $s[n]$, where $n = xT$ is a sufficiently fine spatial sampling of the source function
(2) Zero pad $s[n]$
(3) Compute the DFT; $H(\Omega) = \mathrm{DFT}\{s[n]\}$
(4) Rescale the angle axis $\beta = \lambda\Omega$
(5) Normalize (if desired).

C. Steering

Beam steering is simply shifting the overall response with respect to β, such that

$$H'(\beta) = H(\beta + \beta_s), \tag{7}$$

where β_s is the steering angle. This constant shift in the "transform" domain is equivalent to multiplying by $e^{jk\beta_s x}$ in the "source" domain, i.e.,

$$s'(x) = s(x) e^{jk\beta_s x}. \tag{8}$$

This factor is simply a space-dependent phase shift, or time delay, distributed linearly across the array.

D. Polar cut

When analyzing the one-dimensional directivity of a two-dimensional source, it is useful to reduce the source function to a one-dimensional equivalent, as described in Ref. 1. Under a similar far-field approximation as discussed earlier (where the distance from the array is much larger than the array itself), two-dimensional source $\hat{s}(x,y)$ can be reduced to a one-dimensional equivalent:

$$s(x) \simeq \int \hat{s}(x,y)\, dy. \tag{9}$$

For rectangular elements in a traditional linear array, this integral does not vary over x, so this technique offers little advantage. This method becomes very useful, however, when shaped elements are described in the next section.

E. Discrete array

A source $s(x)$ comprised of a discrete array of identical elements, shown in Fig. 2(a), can be treated as an infinite number of copies of the element source function $s_0(x)$ multiplied by an overall aperture function $w(x)$, which is generally rectangular:

$$s(x) = s_0(x) * \left(w(x) \cdot \sum_{n=-\infty}^{\infty} \delta(x - x_n) \right), \tag{10}$$

where x_n is the location of the nth element, and the asterisk denotes convolution. For a periodic array, where $x_n = nd$, the far-field response $H(\beta)$, given by the Fourier transform of the source function $s(x)$ is

$$H(\beta) = S_0(\beta) \cdot \left(W(\beta) * \sum_{m=-\infty}^{\infty} \delta\left(\beta - \frac{m\lambda}{d} \right) \right). \tag{11}$$

This can be conveniently written as the product of two directivity functions, $H_1(\beta)$ and $H_2(\beta)$:

$$H(\beta) = H_1(\beta) H_2(\beta), \tag{12}$$

with $H_1(\beta) = S_0(\beta)$ and $H_2(\beta)$ equal to the terms in parentheses. In this study, only the quantity $H_1(\beta)$ is of interest, as it is wholly dependent on the individual element characteristics.

An example array with rectangular elements is shown in Fig. 2(a). Here, the rectangular elements have width a and the overall array has a width of D. The normalized responses from these components, plotted in Fig. 2(b) are

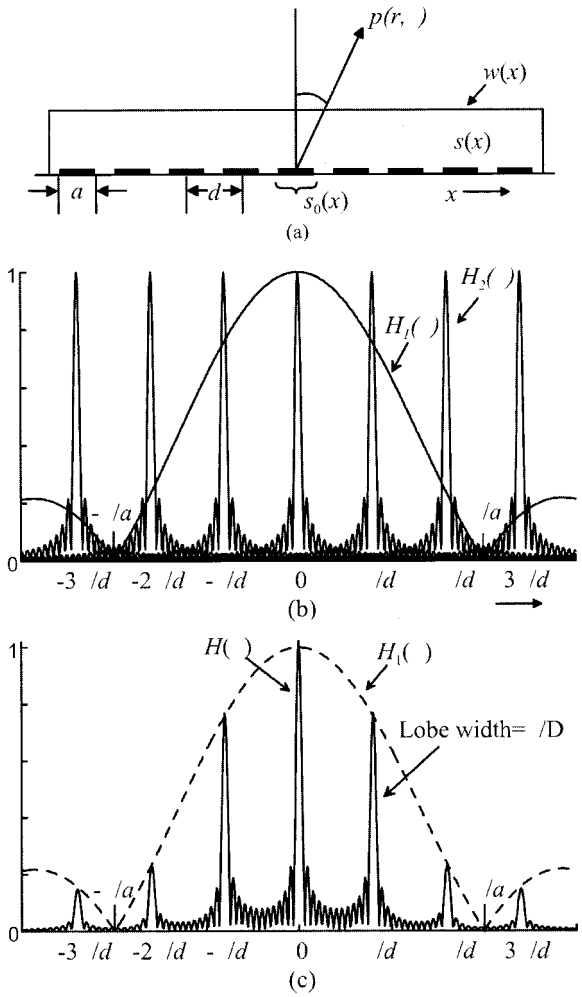

FIG. 2. A typical linear array, with rectangular elements. The physical components of the array, including the elements of width a, interelement spacing d, and overall array size D, are shown in (a). The contributions of the directivity function due to the element size and overall array size are shown in (b). The final directivity function $H(\beta)$ is shown in (c). Recall that $\beta=\sin\theta$.

$$s_0(x)=\mathrm{rect}(a)\Leftrightarrow H_1(\beta)=\mathrm{sinc}(\pi a\beta/\lambda), \tag{13}$$

$$w(x)=\mathrm{rect}('D)\Leftrightarrow W(\beta)=\mathrm{sinc}(\pi D\beta/\lambda). \tag{14}$$

The rectangular function $\mathrm{rect}(a)$ is unity for $-a/2\leqslant x\leqslant a/2$ and zero otherwise, and $\mathrm{sinc}(x)=\sin(x)/x$. The constant interelement spacing of d creates periodic lobes at intervals d/λ in $H_2(\beta)$. The final response $H(\beta)$ is shown in Fig. 2(c). Only the interval $-1\leqslant\beta\leqslant 1$ maps to physical space, so this interval is usually termed the *visible region*. Any additional lobes present in this region are termed *grating lobes*.

This result illustrates two important intuitive points:

(i) The far-field response consists of an infinite set of copies of the overall aperture response $W(\beta)$, spaced by λ/d.

(ii) This total response is then modulated by an *element* response, or the directivity envelope, $H_1(\beta)$.

Thus, in the ''source'' domain, the individual element response influences the overall response of the array in the transform domain, while the overall window in the source domain affects the individual elements in the transform domain.

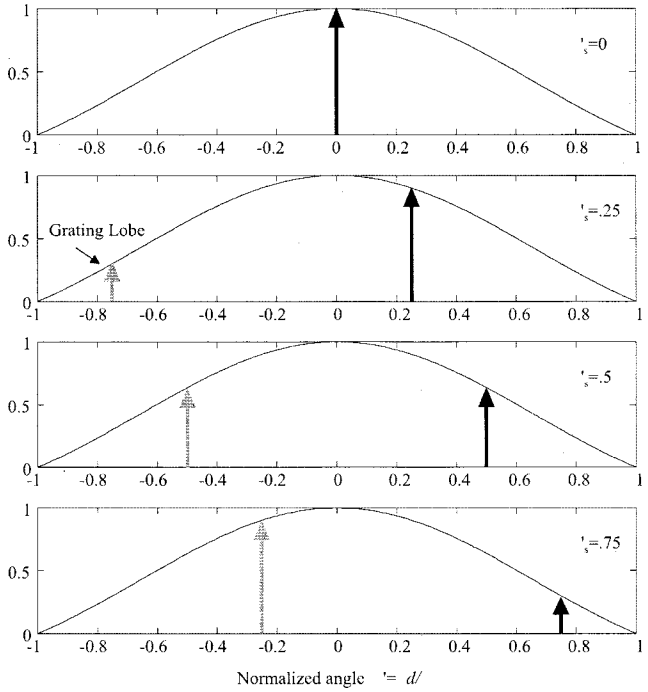

FIG. 3. The directivity of a dense array with element size a equal to the element spacing d. The plots show the changing position and amplitude of the main lobe and grating lobe as the beam is steered. Notice that the magnitude of the grating lobe is equal to that of the main lobe when $\beta_s=\lambda/2a$.

F. Dense arrays

In many applications, it is desirable to maximize sensitivity per unit length of the array, which necessitates the maximization of the density of the array. In a traditional linear array, this is accomplished by making the interelement spacing d equal as close as possible to the element size a. This type of array may be called a *dense array*.

For an array with element size a equal to its interelement spacing d, the grating lobes in an unsteered beam are coincident with zeros in the directivity envelope $H_1(\beta)$, as shown in the upper plot of Fig. 3.

For clarity, the magnitudes are plotted with respect to a normalized angle $\beta'=\beta d/\lambda$, so that variations in wavelength will simply rescale the horizontal axis, and affect the visible region, not the shape of the response.

As the beam is steered, the grating lobe increases in magnitude, while the main lobe decreases. The main lobe and grating lobe have equal amplitudes when $\beta_s'=1/2$, or equivalently when $\beta_s=\lambda/2a$. This sets a limit on useful steering angle to a small range of angles where $\beta_s<\lambda/2a$.

G. Steering performance

The most important indicators of phased array performance which depend on array geometry are (1) the main lobe magnitude M, (2) the grating lobe magnitude G, and (3) the ratio between the amplitude of the main lobe versus that of the grating lobe $\zeta=M/G$. Recall that the beam width is independent of the element shape, and is simply associated

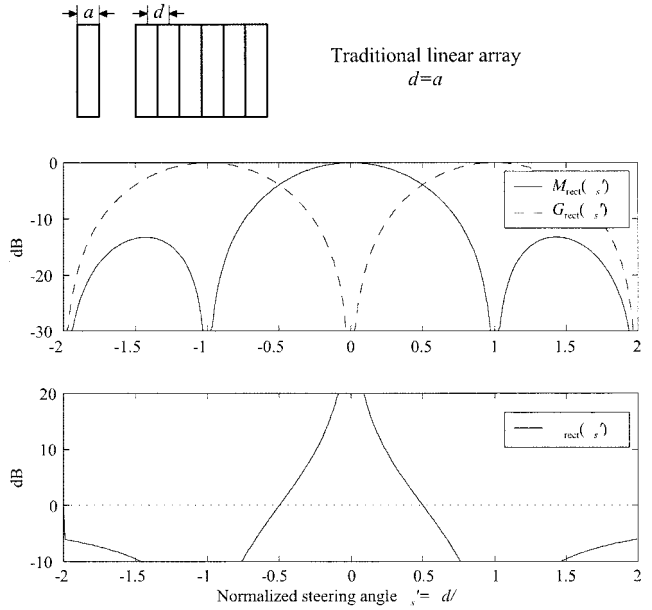

FIG. 4. A rectangular element dense linear array, where $d=a$. The upper plot shows the magnitude of the main lobe M and grating lobe G as a function of normalized steering angle β_s', and the bottom plot shows the ratio ζ of main lobe to grating lobe amplitude. Note that, while the magnitude of the main lobe does not diminish substantially for small angles, the main lobe to grating lobe ratio vanishes quickly for even small steering angles.

with the overall extent of the array D. As the characteristics of interest are due only to elements themselves, an infinitely large array is assumed, so that the lobes are impulses.

For a dense rectangular (traditional linear)array, where $d=a$, the main lobe magnitude M and grating lobe magnitude G as a function of steering angle are

$$M_{\mathrm{rect}}(\beta_s)=\mathrm{sinc}\,(\pi\beta_s a/\lambda), \tag{15}$$

$$G_{\mathrm{rect}}(\beta_s)=\mathrm{sinc}\,(\pi(\beta_s a/\lambda\pm 1)), \tag{16}$$

and the ratio ζ of the main lobe to grating lobe is

$$\zeta_{\mathrm{rect}}(\beta_s)=\frac{\mathrm{sinc}\,(\pi\beta_s a/\lambda)}{\mathrm{sinc}\,(\pi(\beta_s a/\lambda\pm 1))}. \tag{17}$$

In normalized angular coordinates $\beta_s'=\beta_s d/\lambda$,

$$M_{\mathrm{rect}}(\beta_s')=\mathrm{sinc}\,(\pi\beta_s'), \tag{18}$$

$$G_{\mathrm{rect}}(\beta_s')=\mathrm{sinc}\,(\pi(\beta_s'\pm 1)), \tag{19}$$

$$\zeta_{\mathrm{rect}}(\beta_s')=\frac{\mathrm{sinc}\,(\pi\beta_s')}{\mathrm{sinc}\,(\pi(\beta_s'\pm 1))}. \tag{20}$$

These results (in decibels) are plotted in Fig. 4. Note that, while the main lobe amplitude is strong for modest angles, the ratio ζ diminishes very quickly as the beam is steered. An improved phased array system would have a more uniform main lobe response and lobe ratio ζ for a desired steering sector. As these functions are wholly dependent on the element source function $s_0(x)$, this source function can be tailored to improve the lobe ratio ζ.

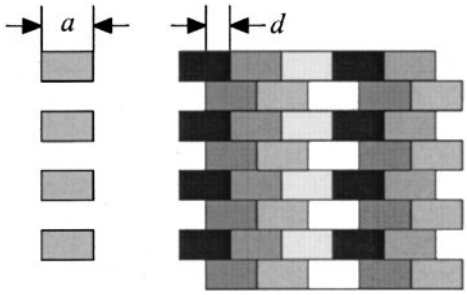

FIG. 5. Simple staggered element pattern. For clarity, each vertical element is shaded differently.

III. OVERSIZED ELEMENTS: STAGGERED ARRAYS

One way of improving the lobe ratio ζ is to narrow the directivity envelope $H_1(\beta)$ of the array. Narrowing this response will somewhat limit the maximum steering angle, but will further suppress grating lobes which occur at large angles. This necessitates increasing the element size compared to the interelement spacing. One of the ways to accomplish this in a planar array is to allow the interleaving or staggering of elements.

A. Staggered rectangular elements

A simple staggered array pattern is shown in Fig. 5. In this case, the individual element is a vertical set of rectangular apertures of width a driven as one unit. Because the elements are effectively overlapping, the element width is twice the interelement spacing d. Taking a polar cut along the x direction shows that the equivalent 1-D source function $s_0(x)$ is simply a rectangular window of width a.

The main and grating lobe magnitudes M and G, and their ratio ζ, are shown in Fig. 6. Clearly, this technique does

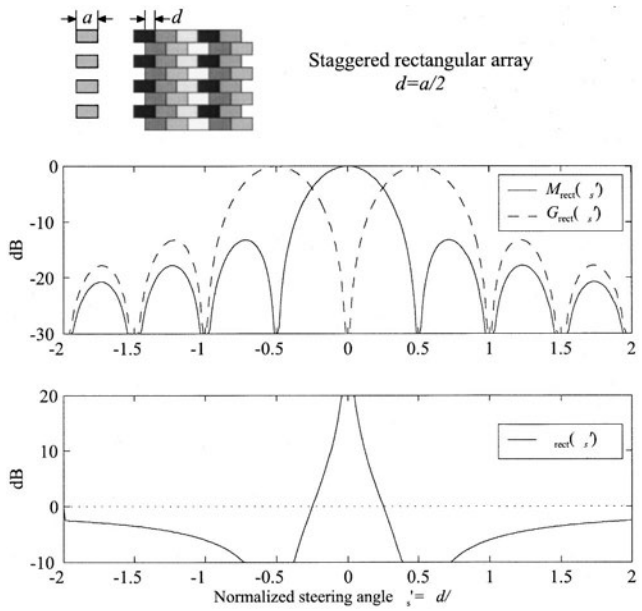

FIG. 6. The lobe magnitudes and main to grating lobe magnitude ζ for a rectangular staggered array, with interelement spacing equal to half the element width ($d=a/2$). Note that performance is diminished compared to the traditional linear array, both in main lobe magnitude and main to grating lobe ratio.

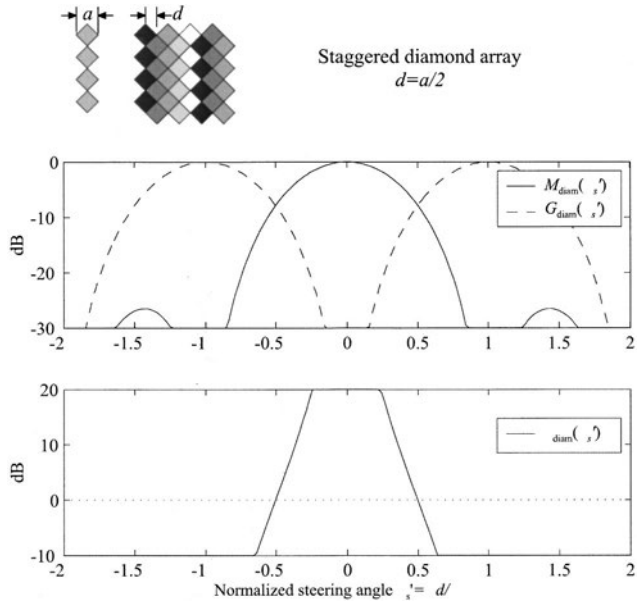

FIG. 7. A staggered linear array of diamond-shaped elements, with their more gradual taper, leads to a more uniform directivity envelope than the staggered rectangle array. There is also substantial improvement in main to grating lobe ratio ζ.

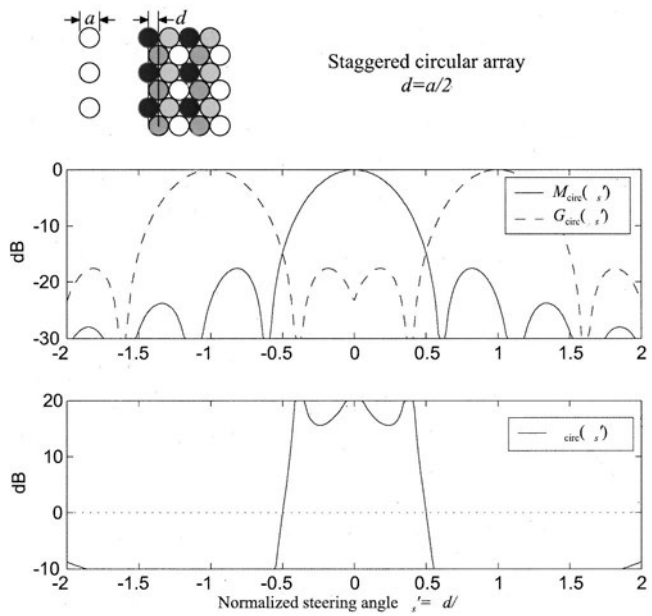

FIG. 8. The lobe magnitudes and main to grating lobe ratio ζ for a staggered circular array. While ζ is generally improved compared to that in the diamond array, the main lobe amplitude M is less uniform across steer angle.

narrow the array envelope, but does not improve the ratio ζ, due to the large ''side lobes'' now present in the directivity envelope. Furthermore, this technique significantly reduces the magnitude of the main lobe for even modest steering angles, which is of course undesirable.

B. Staggered diamond elements

The diamond pattern of array elements shown in Fig. 7 is worth considering, as it has a natural tightly packed configuration, and, being very similar to the rectangular array, is convenient to fabricate. Each element can be described as a triangular source function, where $\mathrm{tri}(a) = (-(2/a)x+1)\,\mathrm{sign}(x)$ for $-a/2 \leqslant x \leqslant a/2$, and zero otherwise. Its corresponding response is (with a scaling of the abscissa) that of the staggered rectangular response squared:

$$s_{\mathrm{diam}}(x) = \mathrm{tri}(a), \tag{21}$$

$$S_{\mathrm{diam}}(\beta) = [\mathrm{sinc}(\pi\beta_s a/2\lambda)]^2. \tag{22}$$

The more gentle taper in the element source function leads to a more uniform directivity envelope, leading to less attenuation of the main lobe across steering angle, as well as improvement in the lobe ratio ζ.

C. Staggered circular elements

The staggered circular element array, like the diamond element array, creates a more uniform directivity envelope due to its more gentle element taper. For this array, the source function and its response for a circular element of diameter a are simply

$$s_{\mathrm{circ}}(x) = \mathrm{circ}(a), \tag{23}$$

$$S_{\mathrm{circ}}(\beta) = \frac{J_1(\pi\beta a/\lambda)}{\pi\beta a/\lambda}, \tag{24}$$

where $\mathrm{circ}(a) = \sqrt{a^2/4 - x^2}$ for $-a/2 \leqslant x \leqslant a/2$ and zero otherwise, and J_1 is the Bessel function of the first kind.

In this case, the element width a is again twice the interelement spacing d. The large element size narrows the array response to an extent, but the more gradual taper of the circular aperture lowers side-lobe magnitude, and thus more effectively suppresses the grating lobe. This is clearly seen in the lower graph of Fig. 8.

For moderate steering angles ($|\beta_s'| < 0.4$), the lobe ratio ζ is superior to that of a rectangular or diamond shape, albeit at the expense of an attenuated main lobe. Here, the -3 dB main lobe angle is at $|\beta_s'| \approx 0.26$, compared to the corresponding $|\beta_s'| \approx 0.32$ for the diamond shape, or $|\beta_s'| \approx 0.45$ for a traditional rectangular element. In those applications for which the per channel cost is of greater concern than sensitivity, this can be a worthwhile tradeoff. However, for many applications where maximum sensitivity is important, this solution is inadequate. In the next section, an optimal element shape is developed not only to suppress grating lobes but also to maximize main lobe amplitude.

IV. OPTIMAL ELEMENTS

From the previous examples, it is shown that control of element shape, coupled with the use of staggered elements, improves the ratio of main lobe to grating lobe amplitude, at the expense of diminished main lobe amplitude. An optimal element shape would produce a directivity envelope corresponding to a rectangular window function, which is unity for $|\beta| < \beta_0$, and zero otherwise. For steering angles smaller than β_0, the main lobe would be unattenuated, but the grating lobe (at β_G) would be fully suppressed, so long as $|\beta_G| > \beta_0$. The corresponding element shape which produces such a function is, of course, the sinc function.

The difficulty in using the sinc function as an element shape lies in both its infinite spatial extent and the require-

ment of signal inversion to reproduce negative swings. Limiting the size of the element will diminish the sharpness of the directivity envelope, but through creative element design this effect can be minimized. Recall that because of the polar cut approximation in the one-dimensional array, the element source function of interest is actually the *vertically integrated* shape of the element, providing a great deal of flexibility in designing its actual shape. As far as the far-field approximation holds, the element can be offset or distributed as desired in the vertical dimension, allowing interleaving or other layout advantages.

The requirement of inverted areas of the elements may, depending on the specifics of the transducer, increase transducer complexity, and add challenges in signal routing. However, a signal inversion is usually easy to implement compared to generating a new delay line channel. In many cases, the electrical connections to the inverted elements can simply be reversed.

A. Altering the elements

The techniques presented in this study prescribe various element source functions, which can be implemented in a variety of ways. Most convenient for acoustic transducers are the following:

1. Element shading

It may be possible, depending on the application, to shade the response of each element, so that while the element itself maintains a traditional rectangular or other convenient shape, the source function $s_0(x)$ is no longer a simple rectangular aperture. For ultrasonic transducers, this could correspond to adding gradients in the thickness, density, or resonance mechanism along the vibrating element, or by deploying an acoustic filter to modify $s_0(x)$.

2. Element shaping

According to the polar cut approximation, an element driven uniformly will have an equivalent source function equal to the transverse integral across the element. Thus, an element can be shaped as needed to provide the desired response. This is most appropriate for a one-dimensional array.

Proper selection of shapes allows the use of staggered elements which are necessary for narrowing the array envelope. Care must be taken with effects along the vertical (nonazimuthal) direction, as the elements are no longer uniform along this axis; however, as long as this dimension is much larger than the element width, creating a very (vertically) narrow main lobe, these effects should be small.

3. Matrix approximation

In some transducer designs, such as diced-piezoelectric crystals or small microphones, it is inconvenient to shape the individual elements accurately. As an alternative, groups of small subelements may be gathered and cross-coupled to approximate a larger element having the desired source function. This may require a more complex interconnection scheme, but the reduced delay channel count may make this worthwhile.

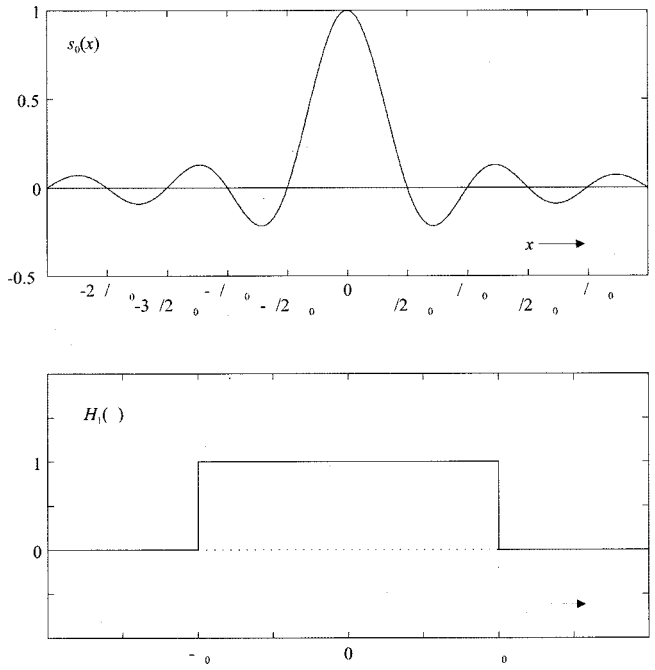

FIG. 9. An example of a sinc-type array element. The upper plot shows the element source function $s_{\text{sinc}}(x)=\text{sinc}\,(2\pi\beta_0 x/\lambda)$, which (if it were infinitely long) would produce the array envelope $H_{1,\text{sinc}}(\beta)=\text{rect}\,(2\beta_0)$, shown in the lower plot. By using the array envelope to limit maximum steering angle to β_0, grating lobes can be suppressed, allowing the relaxing of the interelement spacing restriction.

A practical implementation may use some combination of these methods. For a one-dimensional array, it is probably most straightforward to construct uniformly driven, specially shaped array elements.

B. Optimized element: Windowed sinc

The ideal element shape for producing an array envelope with cutoff angle β_0 is the sinc function, given by

$$s_{\text{sinc}}(x)=\text{sinc}\,(2\pi\beta_0 x/\lambda), \tag{25}$$

which has the corresponding response of

$$H_{1,\text{sinc}}(\beta)=\text{rect}\,(2\beta_0). \tag{26}$$

As shown in Fig. 9, the parameter β_0 corresponds to the dilation of the sinc function in the upper graph, whose zero crossings are at integer multiples of $\lambda/2\pi\beta_0$.

Recall that grating lobes are spaced at angles $\beta_G=\lambda/d$, so to avoid grating lobes completely, the grating lobes must be located at $|\beta_G|>\beta_0$, or

$$d<\frac{\lambda}{2\beta_0}. \tag{27}$$

Since $\beta_0<1$, this interelement spacing constraint is always less stringent than that of a traditional linear array. In fact, if the maximum steering angle is limited to ± 30 degrees ($\beta_0=0.5$), the interelement spacing, and therefore the required number of elements, can be decreased by half, without introducing grating lobes.

Because this type of element is not physically realizable, a windowed sinc function,

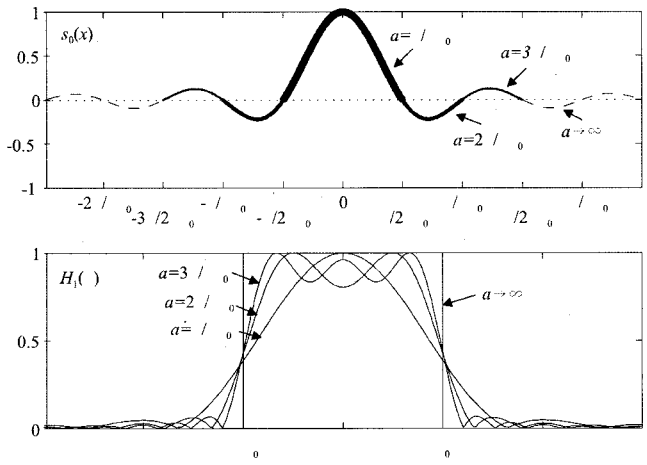

FIG. 10. Three proposed element source functions $s_0(x)$, each of which is a windowed sinc function, are shown in the upper graph. Below, their resulting array envelopes are shown. With a larger element size, the corresponding response approaches an ideal rectangular function.

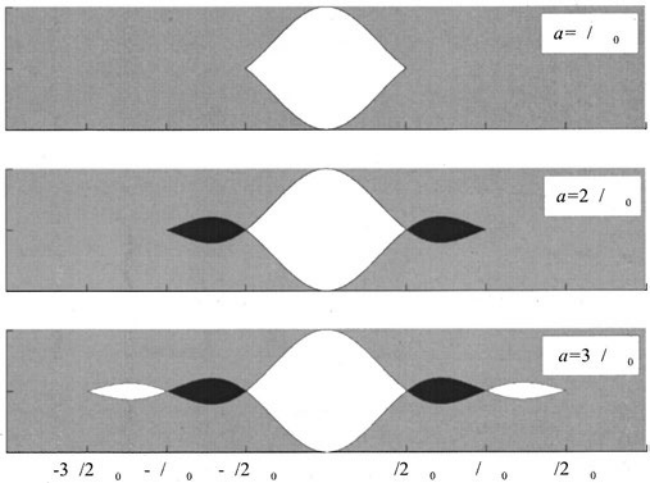

FIG. 11. Three sizes of the optimal sinc-shaped element are shown. The vertical dimension, having no substantial impact on beam steering, is in arbitrary units. The black areas, representing negative swings in the sinc function, are driven inverted with respect to the white areas.

$$s_{\mathrm{wsinc}}(x)=\mathrm{sinc}\,(2\pi\beta_0 x/\lambda)\cdot\mathrm{rect}\,a, \tag{28}$$

which is truncated to width a, may be used instead. This has the corresponding response:

$$S_{\mathrm{wsinc}}(\beta)=\mathrm{rect}\,(2\beta_0)*\mathrm{sinc}\,(\pi a\beta/\lambda). \tag{29}$$

The limitation of the length of the array element leads to a reduction in sharpness of the directivity envelope cutoff, as well as slight ripples in the main lobe magnitude for small steering angles. Of course, one could also use other window shapes (such as Chebyshev) to adjust these effects.

As it is logical to include an integral number of ''lobes'' (areas between zero crossings) in the element function, we can consider element lengths $a_0=\lambda/\pi\beta_0$, $a_1=2\lambda/\pi\beta_0$, and $a_2=3\lambda/\pi\beta_0$. These elements, with their corresponding response envelopes, are shown in Fig. 10.

C. Shaping elements

As discussed in an earlier section, the proposed element source function $s_0(x)$ can be obtained in several ways from a two-dimensional element, so long as

$$\int \hat{s}_0(x,y)\,dy=\mathrm{sinc}\,(2\pi\beta_0 x/\lambda)\cdot\mathrm{rect}\,(a).$$

The most straightforward method is to simply shape the elements in a two-dimensional plane as

$$\hat{s}_0(x,y)=\begin{cases}1 & \text{for } |y|\leqslant \mathrm{sinc}\,(2\pi\beta_0 x/\lambda)\cdot\mathrm{rect}\,(a)\\ 0 & \text{otherwise}\end{cases}. \tag{30}$$

This maintains symmetry in the vertical direction, and leads to a straightforward implementation. The element shapes for various a are shown in Fig. 11. While any desired length a can be used, it is logical to use element lengths which are bounded by zero crossings, as each of these areas specify discrete subelements.

Note that an arbitrary offset $y=v(x)$ can be added along the y direction without impacting the resulting integral because the response is integrated over the vertical direction. This allows a ''warping'' suitable for constructing staggered arrays. If desired, the shape can be reflected across the x axis, or subdivided into smaller segments, which can then be individually moved in the y direction. The impact of these transformations should be very small, even in along the elevation dimension, as long as the far-field approximation holds and the overall y dimension is much larger than the element size. Issues related to nonazimuthal effects will be explored in a later section.

D. Choice of element width

As has been discussed, the elimination of grating lobes requires an interelement spacing $d<\lambda/2\beta_0$. Note that the zero crossings of the element's sinc function are spaced in a manner proportional to λ/β_0. Therefore, the maximum allowable interelement spacing relative to the dilation of the source (sinc) function will be constant. In other words, any changes in the ratio λ/β_0 will simply rescale the x axis of the entire array, including the element itself and the interelement spacing, and limiting steerable angle.

In order to minimize the required number of elements by maximizing interelement spacing, the spacing $d=\lambda/2\beta_0$ can be used, which occurs slightly after the third zero crossing in the sinc function. This indicates that a convenient element width would be $a=3\lambda/\pi\beta_0$. In order to panel elements cleanly, d can be reduced slightly to $d=3\lambda/2\pi\beta_0$. The final array is shown in Fig. 12.

V. PERFORMANCE

The array proposed in Fig. 12 has an interelement spacing of

$$d=\frac{3\lambda}{2\pi\beta_0}, \tag{31}$$

which corresponds to a limiting steering angle of

$$\beta_0=\frac{3\lambda}{2\pi d}\approx\frac{\lambda}{2d}. \tag{32}$$

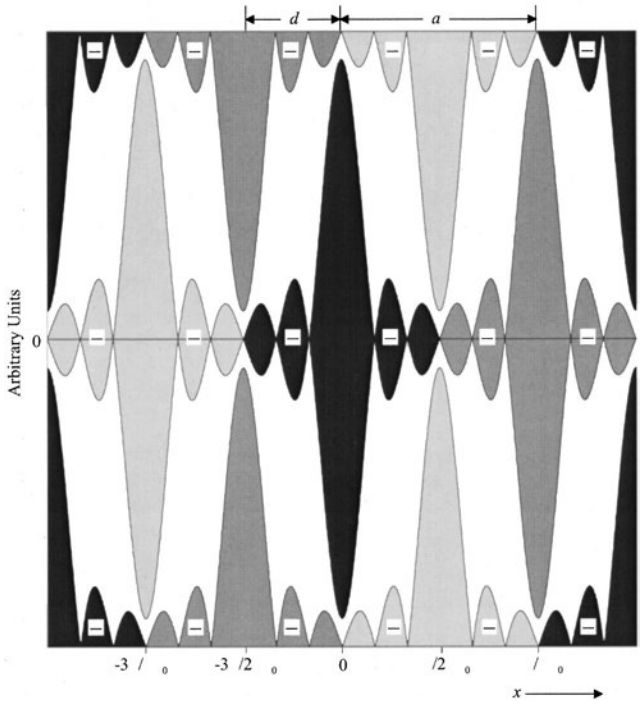

FIG. 12. Proposed array pattern, consisting of elements shaped as sinc functions. Each element is shaded differently to show their separation. Those regions whose excitation polarity is to be inverted are marked with a "−" sign. The horizontal axis is scaled relative to the ratio λ/β_0, and the vertical axis is of arbitrary units.

The element width is taken as $a=d/2$, as in the earlier interleaved designs. The resulting main lobe amplitude M_{sinc} and main lobe to grating lobe ratio G_{sinc} are shown Fig. 13. Clearly the array optimization has successfully suppressed the grating lobe for limited steering angles, while maintaining a near-constant main lobe amplitude.

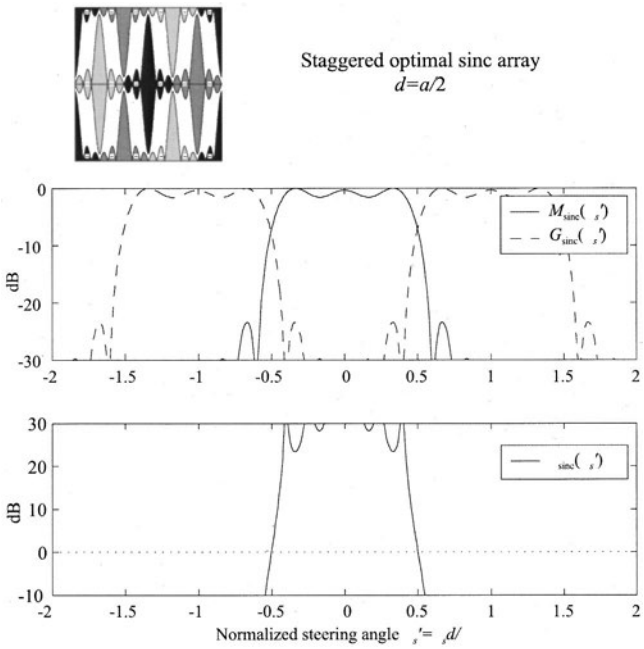

FIG. 13. Magnitude of main lobe, and main to grating lobe ratio, for the optimal array shown in Fig. 12. Steering angle is effectively limited to $|\beta_s'|<0.5$, over which the main lobe amplitude is nearly constant, and the grating lobe is effectively suppressed.

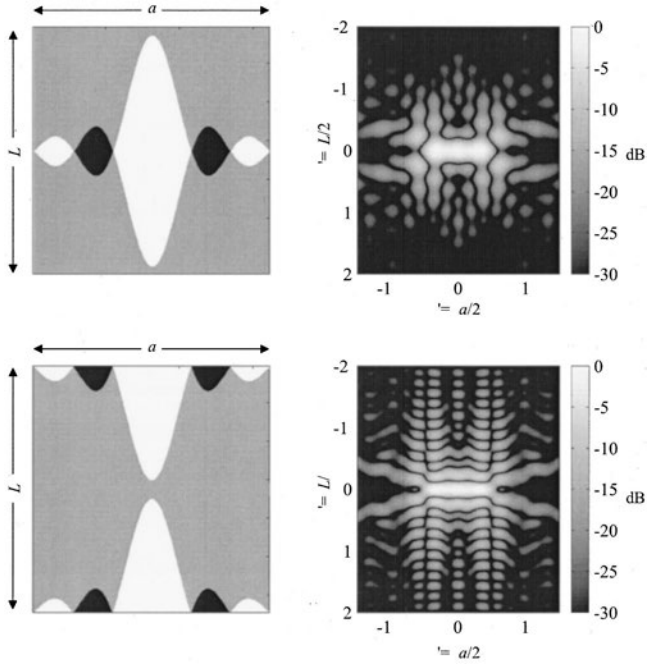

FIG. 14. The two styles of sinc elements are shown, with their respective responses, as a function of normalized angle. The black regions are driven inverted. For consistency with earlier figures, they are plotted against the normalized angles $\beta'=\beta a/2\lambda$ and $\gamma'=\gamma L/2\lambda$, where $a=2d$.

As with most phased array designs, this type of design must only meet the criteria for the smallest wavelength it is designed to handle, that is, for $\lambda \geq 2d\beta_0$. Any increase in λ simply increases the steering cutoff angle.

VI. TWO-DIMENSIONAL BEAM CHARACTERISTICS

From the previous section, the directivity envelope in the azimuthal plane approximates a rectangular function limited by steer angle β_0. Depending on the particular selection of tiling geometry, the vertical pattern of the envelope can vary significantly. For this reason, it is important that the performance, in particular the presence of spurious lobes, is assessed in the vertical plane.[13]

The analysis for the two-dimensional array is much like that for the one-dimensional array, but using a two-dimensional Fourier transform. The vertical size of the element can be defined as L, and elevation angle $\gamma=\sin\phi$.

Recall that, because of the polar cut approximation, the vertical dimension can be scaled, offset, or moved as desired, as long as the far-field approximation holds and the elements do not overlap. This allows an unlimited number of element tiling methods, although the most important has compact size, such as that shown in Fig. 12.

The linear array proposed in the previous section contains two types of elements, both with equivalent azimuthal responses. A two-dimensional analysis shows the expected azimuthal cutoff at $|\beta_0'|=0.5$ in Fig. 14, but the vertical characteristics may give rise to spurious vertical lobes if the main lobe is not sufficiently narrow. Because the vertical dimension L of the element makes equal contributions to the main

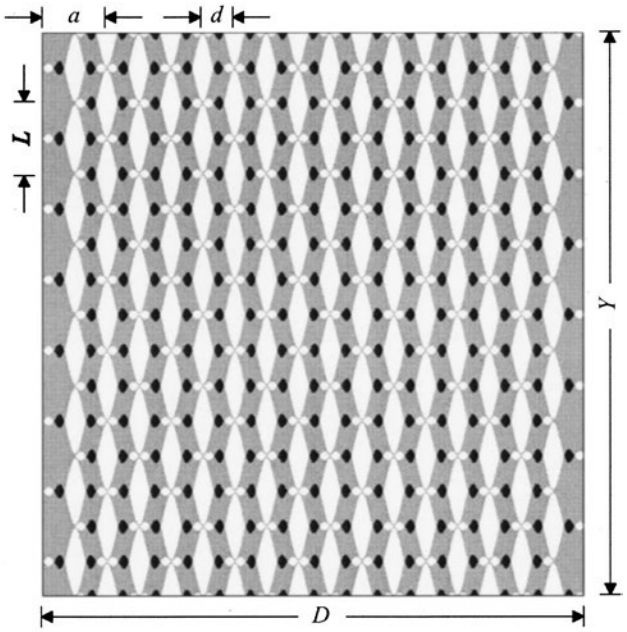

FIG. 15. The proposed linear array, using staggered sinc elements. Because the vertical dimension Y is much larger than the element height L, the main lobe will be sufficiently narrow to mitigate the presence of vertical side lobes. The interelement spacing, as before, is one-half the element size, in both the horizontal and vertical dimensions.

lobe height and the vertical envelope, simply scaling this parameter will not affect the presence of vertical lobes. Instead, if a two-dimensional staggered array of sinc elements, such as the one shown in Fig. 15, is used, no vertical sidelobes will develop. The vertical dimension Y of the array is much larger than the element, so the lobe height will be much narrower than the directivity envelope. Since the array is steered only in the azimuthal direction, grating lobes will never appear in the vertical direction.

VII. CONCLUSIONS

A unique and potentially useful method of phased array design has been presented, which puts particular emphasis on the shape of the individual elements in order to naturally suppress grating lobes. Much like a shaped or shaded array mitigates sidelobes, careful design of the constituent element shapes can naturally mitigate grating lobes, without detrimental effects to the main lobe.

By using properly shaped elements in staggered arrays, the minimum interelement spacing requirement can be smoothly exchanged for maximum steering angle. In many instances, this may lead to a substantial reduction in delay-line channels for a phased array system, as is particularly valuable in continuous-wave systems.

One limitation may be the cost and complexity of physically fabricating the proper transducer elements, or in inverting some subelements. While prohibitive for some applications, particularly in very-high-frequency ultrasound, there are many applications for which this may be a suitable and useful technique.

ACKNOWLEDGMENTS

This paper is a result of independent graduate term project. FJP would like to thank Professor Barry Vercoe and the Music, Mind & Machine Group for their helpful comments and general support. SCW would like to acknowledge the National Science Foundation for their encouragement (CMS-9903535).

[1] B. D. Steinberg, *Principles of Aperture and Array System Design* (Wiley, New York, 1976).
[2] S. C. Wooh and Y. Shi, "Optimum beam steering of linear phased arrays," Wave Motion **29**, 245–265 (1999).
[3] D. H. Turnbull and F. S. Foster, "Beam steering with pulsed two-dimensional transducer arrays," IEEE Trans. Ultrason. Ferroelectr. Freq. Control **38**(4), 320–333 (1991).
[4] B. D. Steinberg, "Comparison between the peak sidelobe of the random array and algorithmically designed aperiodic arrays," IEEE Trans. Antennas Propag. **AP-21**, 366–369 (1973).
[5] S. S. Brunke and G. R. Lockwood, "Broad-bandwidth radiation patterns of sparse two-dimensional vernier arrays," IEEE Trans. Ultrason. Ferroelectr. Freq. Control **44**(5), 1101–1109 (1997).
[6] S. W. Smith, H. G. Pavy, and O. T. von Ramm, "High-speed ultrasound volumetric imaging system—Part I: Transducer design and beam steering," IEEE Trans. Ultrason. Ferroelectr. Freq. Control **38**(2), 100–108 (1991).
[7] G. R. Lockwood, P. C. Li, M. O'Donnell, and F. S. Foster, "Optimizing the radiation pattern of sparse periodic linear arrays," IEEE Trans. Ultrason. Ferroelectr. Freq. Control **43**(1), 15–19 (1996).
[8] G. R. Lockwood and F. S. Foster, "Optimizing the radiation pattern of periodic two-dimensional arrays," IEEE Trans. Ultrason. Ferroelectr. Freq. Control **43**(1), 15–19 (1996).
[9] O. T. von Ramm and S. Smith, "Beam steering with linear arrays," IEEE Trans. Biomed. Eng. **BME-30**(8), 438–452 (1983).
[10] F. J. Pompei, "The use of airborne ultrasound for generating audible sound beams," J. Audio Eng. Soc. **47**(9), 726–731 (1999).
[11] S. C. Wooh and Y. Shi, "Influence of phased array element size on beam steering behavior," Ultrasonics **36**, 737–749 (1998).
[12] S. P. Skobelev, "Methods of constructing optimum phased-array antennas for limited field of view," IEEE Antennas Propag. Mag. **40**(2), 39–50 (1998).
[13] S. C. Wooh and Y. Shi, "Three-dimensional beam directivity of phase-steered ultrasound," J. Acoust. Soc. Am. **105**, 3275–3282 (1999).